

## Anomalous Transport and Diffusion in Percolation Systems

Armin Bunde,<sup>1</sup> Paul Heitjans,<sup>2</sup> Sylvio Indris,<sup>3</sup> Jan W. Kantelhardt,<sup>4</sup> Markus Ulrich<sup>1</sup>

<sup>1</sup>Universität Giessen, Institut für Theoretische Physik, Germany

<sup>2</sup>Leibniz Universität Hannover, Institut für Physikalische Chemie, Germany

<sup>3</sup>Forschungszentrum Karlsruhe, Institut für Nanotechnologie, Germany

<sup>4</sup>Universität Halle, Institut für Physik, Germany

Corresponding author:

Armin Bunde

Universität Giessen

D-35392 Giessen

bunde@physik.uni-giessen.de

### Abstract

Many disordered systems can be modelled by percolation. Applications of this standard model range from amorphous and porous media to composites, branched polymers, gels and complex ionic conductors. In this brief review we give a short introduction to percolation theory and describe applications in materials science. We start with the structural properties of percolation clusters and their substructures. Then we turn to their dynamical properties and discuss the way the laws of diffusion and conduction are modified on these structures. Finally, we review applications of the percolation concept for transport in various kinds of heterogeneous ionic conductors.

### 1. The percolation transition

Percolation represents a standard model for a structurally disordered system with a wide range of applications [1-3]. In Sections 1 to 3 we give a brief introduction into percolation theory. For brevity, we skip references to most original works here and instead refer to reviews [1] and [2]. In Section 4 we discuss applications on heterogeneous ionic conductors.

Let us consider a square lattice, where each site is occupied randomly with probability  $p$  or is empty with probability  $1-p$  (see Fig. 1). Occupied and empty sites may stand for very different physical properties. For illustration, let us assume that the occupied sites are electrical conductors, the empty sites represent insulators, and that electrical current can only flow between nearest-neighbour conductor sites.

At low concentration  $p$ , the conductor sites are either isolated or form small clusters of nearest-neighbour sites. Two conductor sites belong to the same cluster if they are connected by a path of nearest-neighbour conductor sites, and a current can flow between them. At low  $p$  values, the mixture is an insulator, since no conducting path connecting

opposite edges of our lattice exists. At large  $p$  values, on the other hand, many conducting paths between opposite edges exist, where electrical current can flow, and the mixture is a conductor. At some concentration in between, therefore, a threshold concentration  $p_c$  must exist where for the first time an electrical current can percolate from one edge to the other. The threshold concentration is called the percolation threshold, or, since it separates two different phases, the critical concentration.

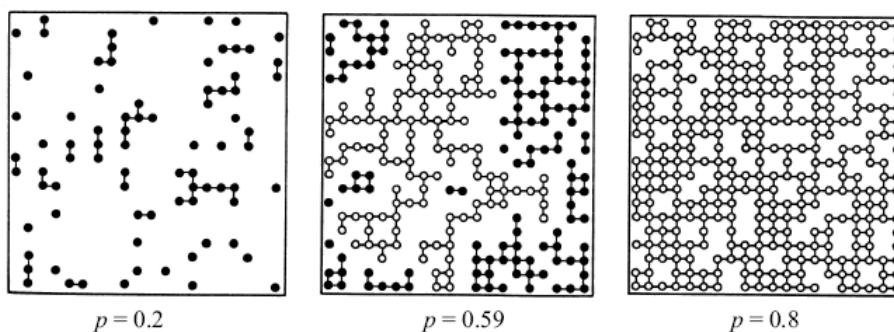


Fig. 1. Site percolation on the square lattice: The small circles represent the occupied sites for three different concentrations:  $p = 0.2$ ,  $0.59$ , and  $0.8$ . Nearest-neighbour cluster sites are connected by lines representing the bonds. Filled circles are used for finite clusters, while open circles mark the large *infinite* cluster.

If the occupied sites are superconductors and the empty sites are conductors,  $p_c$  separates a normal-conducting phase below  $p_c$  from a superconducting phase above  $p_c$ . Another example is a mixture of ferromagnets and paramagnets, where the system changes at  $p_c$  from a paramagnet to a ferromagnet.

In contrast to the more common thermal phase transitions, where the transition between two phases occurs at a critical temperature, the percolation transition described here is a geometrical phase transition, which is characterized by the geometric features of large clusters in the neighbourhood of  $p_c$ . At low values of  $p$  only small clusters of occupied sites exist. When the concentration  $p$  is increased the average size of the clusters increases. At the critical concentration  $p_c$  a large cluster appears which connects opposite edges of the lattice. We call this cluster the *infinite* cluster, since its size diverges in the thermodynamic limit. When  $p$  is increased further the density of the infinite cluster increases, since more and more sites become part of it, and the average size of the *finite* clusters, which do not belong to the infinite cluster, decreases. At  $p = 1$ , trivially, all sites belong to the infinite cluster.

The value of  $p_c$  depends on the details of the lattice and increases, for fixed dimension  $d$  of the lattice, with decreasing coordination number  $z$  of the lattice. For the triangular lattice,  $z = 6$  and  $p_c = 1/2$ , for the square lattice,  $z = 4$  and  $p_c \approx 0.592746$ , while the honeycomb lattice has  $z = 3$  and  $p_c \approx 0.6962$ . For fixed  $z$ ,  $p_c$  decreases if the dimension  $d$  is

enhanced. In both the triangular lattice and the simple cubic lattice we have  $z = 6$ , but  $p_c$  for the simple cubic lattice is considerably smaller,  $p_c \approx 0.3116$ .

So far we have considered site percolation, where the sites of a lattice have been occupied randomly. When the sites are all occupied, but the bonds between them are randomly occupied with probability  $q$ , we speak of bond percolation. Two occupied bonds belong to the same cluster if they are connected by a path of occupied bonds. The critical concentration  $q_c$  of bonds ( $q_c = 1/2$  in the square lattice and  $q_c \approx 0.2488$  in the simple cubic lattice) separates a phase of finite clusters of bonds from a phase with an infinite cluster. Perhaps the most common example of bond percolation in physics is a random resistor network, where the metallic wires in a regular network are cut randomly with probability  $1 - q$ . Here  $q_c$  separates a conductive phase at large  $q$  from an insulating phase at low  $q$ . A possible application of bond percolation in chemistry is the polymerization process, where small branching molecules can form large molecules by activating more and more bonds between them. If the activation probability  $q$  is above the critical concentration, a network of chemical bonds spanning the whole system can be formed, while below  $q_c$  only macromolecules of finite size can be generated. This process is called a sol-gel transition. An example of this gelation process is the boiling of an egg, which at room temperature is liquid and upon heating becomes a more solid-like gel.

The most natural example of percolation is continuum percolation, where the positions of the two components of a random mixture are not restricted to the discrete sites of a regular lattice. As a simple example, consider a sheet of conductive material, with circular holes punched randomly in it. The relevant quantity now is the fraction  $p$  of remaining conductive material. Compared with site and bond percolation, the critical concentration is further decreased:  $p_c \approx 0.312$  for  $d = 2$ , when all circles have the same radius. This picture can easily be generalized to three dimensions, where spherical voids are generated randomly in a cube, and  $p_c \approx 0.034$ . Due to its similarity to Swiss cheese, this model is also called the Swiss cheese model. Similar models, where also the size of the spheres can vary, are used to describe sandstone and other porous materials.

## 2. The fractal structure of percolation clusters near $p_c$

The percolation transition is characterized by the geometrical properties of the clusters near  $p_c$  [1,2]. The probability that a site belongs to the infinite cluster is zero below  $p_c$  and increases above  $p_c$  as

$$P_\infty \sim (p - p_c)^\beta \quad (1)$$

with  $\beta = 5/36$  in  $d = 2$  and  $\beta \approx 0.417$  in  $d = 3$ .

The linear size of the *finite* clusters, below and above  $p_c$ , is characterized by the correlation length  $\xi$ . The correlation length is defined as the mean distance between two sites on the same finite cluster and represents the characteristic length scale in percolation. When  $p$  approaches  $p_c$ ,  $\xi$  increases as

$$\xi \sim |p - p_c|^{-\nu}, \quad (2)$$

with the same exponent  $\nu$  below and above the threshold ( $\nu = 4/3$  in  $d = 2$  and  $\nu \approx 0.875$  in  $d = 3$ ). While  $p_c$  depends explicitly on the type of the lattice, the critical exponents  $\beta$  and  $\nu$  are universal and depend only on the dimension  $d$  of the lattice, but not on the type of the lattice.

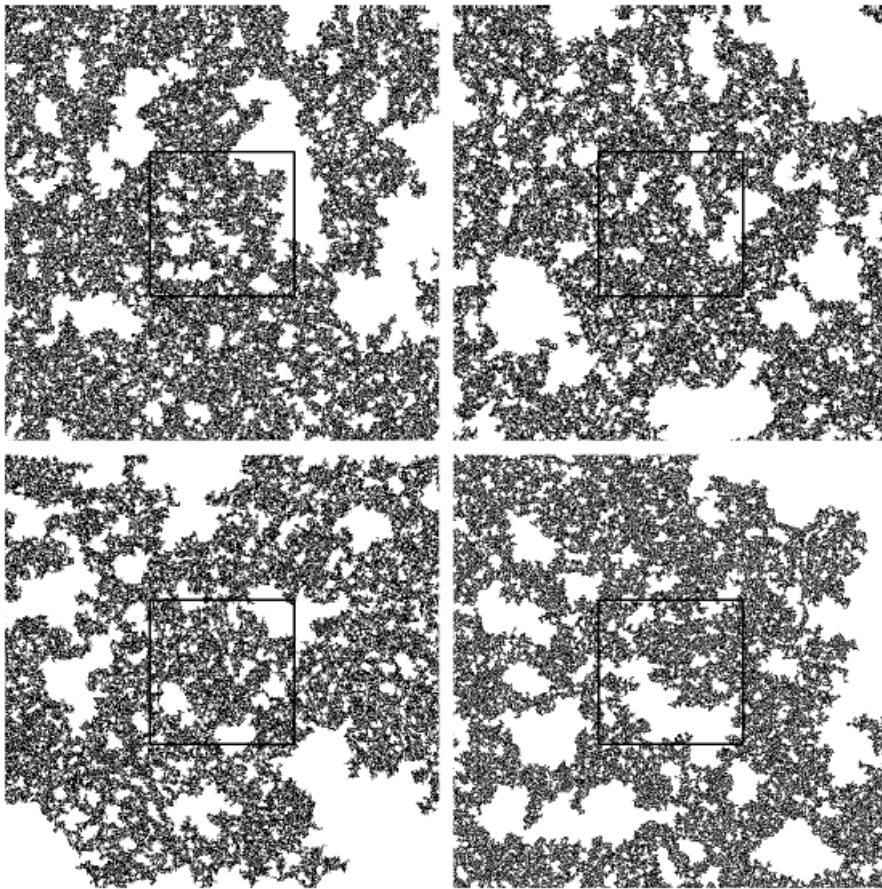


Fig. 2. Four successive magnifications of the incipient infinite cluster that forms at the percolation threshold on the square lattice. Three of the panels are magnifications of the center squares marked by black lines. An educational game is to time how long it takes each player to detect by eye which of the 24 possible orderings is the correct one that arranges the four panels in increasing order of magnification.

For percolation concentrations near  $p_c$  and on length scales smaller than the correlation length  $\xi$ , both the infinite cluster and the finite clusters are self-similar. I.e., if we cut a small part out of a large cluster, magnify it to the original cluster size and compare it with the original, we cannot tell the difference: both look the same. This feature is illustrated in Fig. 2, where a large cluster at  $p_c$  is shown in four different magnifications. We leave it to the reader to find out what is the original and what are the magnifications.

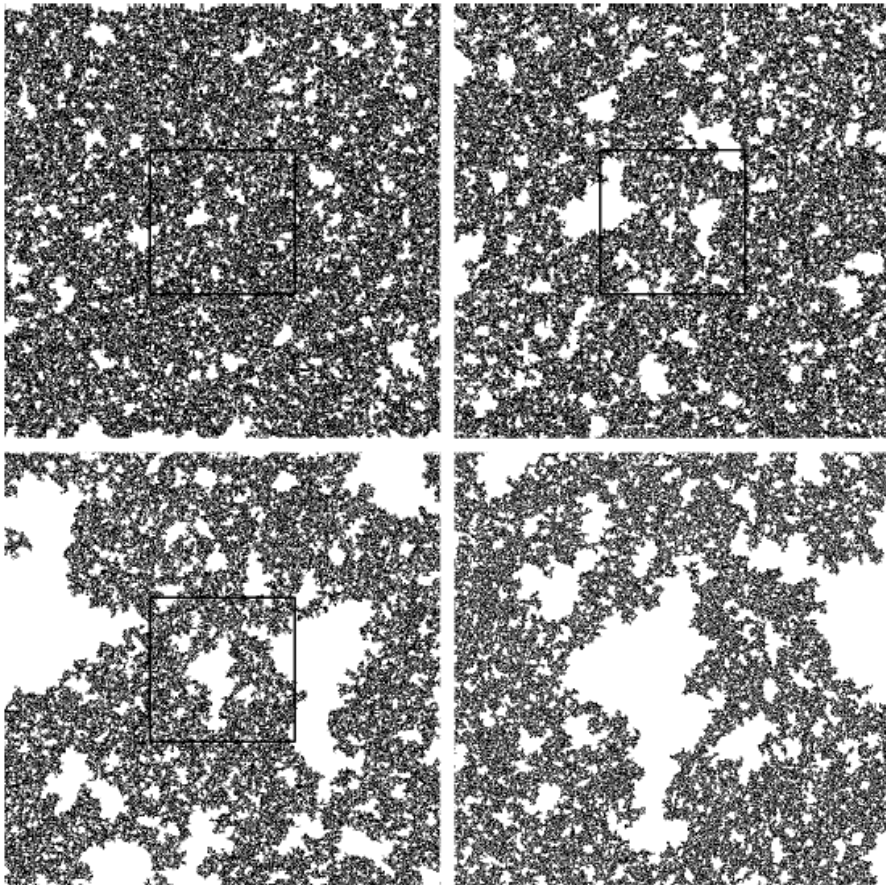


Fig. 3. The same as Fig. 2 except that now the system is slightly (0.3 %) above the percolation threshold and the panels are not scrambled. The upper left picture shows the original and the other pictures are magnifications of the center squares marked by black lines. The correlation length  $\xi$  is approximately equal to the linear size of the third (lower left) picture. When comparing the two lower pictures, the self-similarity at small length scales below  $\xi$  is easy to recognize.

As a consequence of the (non-trivial) self-similarity, the cluster is characterized by a “fractal” dimension, which is smaller than the dimension  $d$  of the embedding lattice. The mean mass of the cluster within a circle of radius  $r$  increases with  $r$  as

$$M(r) \sim r^{d_f}, \quad r \ll \xi, \quad (3)$$

with the fractal dimension  $d_f = 91/48$  in  $d = 2$  and  $d_f \approx 2.5$  in  $d = 3$ . Above  $p_c$  on length scales *larger* than  $\xi$  the infinite cluster can be regarded as a homogeneous system which is composed of many cells of size  $\xi$ . Mathematically, this can be summarized as

$$M(r) \sim \begin{cases} r^{d_f} & \text{if } r \ll \xi, \\ r^d & \text{if } r \gg \xi. \end{cases} \quad (4)$$

Fig. 3 shows a part of the infinite cluster slightly above  $p_c$  ( $p = 1.003 p_c$ ) on different length scales. At large length scales ( $r \gg \xi$ , upper left) the cluster appears homogeneous, while on lower length scales ( $r \ll \xi$ , lower pictures) the cluster is self-similar.

The fractal dimension  $d_f$  can be related to  $\beta$  and  $\nu$  in the following way. Above  $p_c$ , the mass  $M_\infty$  of the infinite cluster in a large lattice of size  $L^d$  is proportional to  $L^d P_\infty$ . On the other hand, this mass is also proportional to the number of unit cells of size  $\xi$ ,  $(L/\xi)^d$ , multiplied by the mass of each cell, which is proportional to  $\xi^{d_f}$ . This yields (with Eqs. (1) and (2))

$$M_\infty \sim L^d P_\infty \sim L^d (p - p_c)^\beta \sim (L/\xi)^d \xi^{d_f} \sim L^d (p - p_c)^{\nu(d-d_f)}, \quad (5)$$

and hence, comparing the exponents of  $(p - p_c)$ ,

$$d_f = d - \frac{\beta}{\nu}. \quad (6)$$

Since  $\beta$  and  $\nu$  are universal exponents,  $d_f$  is also universal.

A fractal percolation cluster is composed of several fractal substructures, which are described by other exponents [1,2]. Imagine applying a voltage between two sites at opposite edges of a metallic percolation cluster: The backbone of the cluster consists of those sites (or bonds) which carry the electric current. The topological distance between both points (also called chemical distance) is the length of the shortest path on the cluster connecting them. The dangling ends are those parts of the cluster which carry no current and are connected to the backbone by a single site only. The red bonds (or singly connected bonds), finally, are those bonds that carry the total current; when they are cut the current flow stops.

The fractal dimension  $d_B$  of the backbone ( $d_B \approx 1.64$  in  $d=2$  and  $d_B \approx 1.86$  in  $d=3$ ) is smaller than the fractal dimension  $d_f$  of the cluster, reflecting the fact that most of the mass of the cluster is concentrated in the dangling ends. On the average, the topological length  $\ell$  of the path between two points on the cluster increases with the Euclidean distance  $r$  between them as  $\ell \sim r^{d_{\min}}$  ( $d_{\min} \approx 1.13$  in  $d=2$  and  $d_{\min} \approx 1.37$  in  $d=3$ ). The fractal dimension of the red bonds  $d_{\text{red}}$  can be deduced from exact analytical arguments: The mean number of red bonds varies with  $p$  as  $n_{\text{red}} \sim (p - p_c)^{-1} \sim \xi^{1/\nu}$ , and the fractal dimension of the red bonds is therefore  $d_{\text{red}} = 1/\nu$ .

It is important for applications that close to the percolation threshold, the exponents are universal and depend neither on the structural details of the lattice (e.g., square or triangular) nor on the type of percolation (site, bond, or continuum), but only on the dimension of the lattice.

### 3. Anomalous Diffusion and Conduction on Percolation Clusters

Next we will focus on the *dynamical* properties of percolation systems, where to each site or bond a physical property such as conductivity is assigned. Due to the fractal nature of the percolation clusters near  $p_c$ , the physical laws of dynamics are changed essentially and become *anomalous*. We start with the infinite percolation cluster at the critical concentration  $p_c$ .

The cluster has loops and dangling ends, and both substructures slow down the motion of a random walker. Due to self-similarity, loops and dangling ends occur on *all* length scales, and therefore the motion of the random walker is slowed down on all length scales. The time  $t$  the walker needs to travel a distance  $R$  is no longer, as in regular systems, proportional to  $R^2$ , but scales as  $t \sim R^{d_w}$ , where  $d_w > 2$  is the fractal dimension of the random walk [1, 2]. For the mean square displacement this yields immediately

$$\langle r^2(t) \rangle \sim t^{2/d_w}. \quad (7)$$

The fractal dimension  $d_w$  is approximately equal to  $3d_f/2$  [4]. For continuum percolation in  $d=3$ ,  $d_w$  is enhanced:  $d_w \approx 4.2$  [5]. In general,  $d_w$  cannot be calculated rigorously. Exceptions are linear fractal structures (like self-avoiding walks), where  $d_w = 2d_f$ , or loopless structures. Diffusion processes described by Eq. (7) are generally referred to as anomalous diffusion.

Above  $p_c$ , fractal structures occur only within the correlation length  $\xi(p)$ . Thus the anomalous diffusion law, Eq. (7), occurs only below the corresponding crossover time  $t_\xi \sim \xi^{d_w}$ , which decreases proportional to  $(p - p_c)^{-\nu d_w}$ , if  $p$  is further increased. Above  $t_\xi$ , on large time scales, the random walker explores large length scales where the cluster is homogeneous, and  $\langle r^2(t) \rangle$  follows Fick's law increasing linearly with time  $t$ . Thus,

$$\langle r^2(t) \rangle \sim \begin{cases} t^{2/d_w} & \text{if } t \ll t_\xi, \\ t & \text{if } t \gg t_\xi. \end{cases} \quad (8)$$

The diffusion coefficient defined by  $D = \langle r^2(t) \rangle / 2dt$  is (approximately) related to the dc conductivity  $\sigma_{dc}$  by the Nernst-Einstein equation,

$$\sigma_{dc} = ne^2 D / k_B T, \quad (9)$$

where  $n$  is the density and  $e$  the charge of the diffusing particles. Below  $p_c$ , there is no current between opposite edges of the system, and  $\sigma_{dc} = 0$ . Above  $p_c$ ,  $\sigma_{dc}$  increases by a power law

$$\sigma_{dc} \sim (p - p_c)^\mu, \quad (10)$$

where the critical exponent  $\mu$  is (semi)-universal. For percolation on a lattice,  $\mu$  depends only on  $d$ . For continuum percolation (Swiss cheese model) in  $d = 3$ , however,  $\mu$  is enhanced:  $\mu \approx 2.38$ .

Combining Eqs. (9) and (10), we can obtain the behaviour of the diffusion coefficient  $D$  as a function of  $p - p_c$ . Since only the particles on the infinite cluster contribute to the dc conductivity, we have (from Eq. (1))  $n \sim P_\infty \sim (p - p_c)^\beta$  in Eq. (9). This yields  $D \sim (p - p_c)^{\mu - \beta}$ . Next we use scaling arguments to relate the exponent  $\mu$  to  $d_w$ . Above  $t_\xi$ , the mean square displacement  $\langle r^2(t) \rangle$  behaves as  $\langle r^2(t) \rangle \sim (p - p_c)^{\mu - \beta} t$ , where, for  $t = t_\xi$ , we have  $\langle r^2(t) \rangle \sim \xi^2$ . On the other hand we know that for times below  $t_\xi$  on distances  $r < t_\xi^{1/d_w}$ ,  $\langle r^2(t) \rangle \sim t_\xi^{2/d_w}$ . Equating both relations we obtain immediately  $(p - p_c)^{\mu - \beta} t_\xi \sim t_\xi^{2/d_w}$ . Using  $t_\xi \sim \xi^{d_w} \sim (p - p_c)^{-\nu d_w}$  (from Eq. (2)) we get the relation between  $\mu$  and  $d_w$ ,

$$d_w = 2 + (\mu - \beta) / \nu. \quad (11)$$

#### 4. Application of the Percolation Concept: Heterogeneous Ionic Conductors

Let us now turn to applications of percolation models in materials. A substantial amount of research has concentrated on “dispersed ionic conductors” after the discovery by Liang [6] that insulating fine particles with sizes of the order of  $1\mu\text{m}$ , dispersed in a conductive medium (e. g.  $\text{Al}_2\text{O}_3$  in  $\text{LiI}$ ), can lead to a conductivity enhancement [7]. This effect has been found to arise from the formation of a defective, highly conducting layer following the boundaries between the conducting and the insulating phase [8]. Effectively, the system thus contains three phases. Theoretical studies therefore have focused on suitable three-component impedance network models.

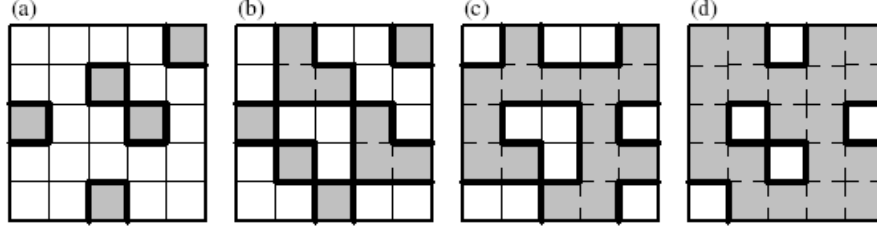


Fig. 4. Illustration of the three-component percolation model for dispersed ionic conductors, for different concentrations  $p$  of the insulating material. The insulator is represented by the grey area, the ionic conductor by the white area. The bonds can be highly conducting bonds (A bonds, bold lines), normal conducting bonds (B bonds, thin lines), or insulating (C bonds, dashed lines). (a)  $p < p'_c$ , (b)  $p = p'_c$ , (c)  $p = p''_c$ , and (d)  $p > p''_c$ .

#### 4.1 Correlated Bond Percolation Model for Dispersed Ionic Conductors

Figure 4 shows a two-dimensional illustration of such composites in a discretized model [9,10]. In its simplest version this model is constructed by randomly selecting a fraction  $p$  of elementary squares on a square lattice, which represent the insulating phase (grey), while the remaining squares are the conducting phase (white). The distribution of both phases leads to a correlated bond percolation model with three types of bonds and associated bond conductances  $\sigma_\alpha$ ;  $\alpha = A, B, C$ ; as defined in Fig. 4. For example, bonds in the boundary between conducting and insulating phases correspond to the highly conducting component (A bonds). This is an extension to the standard bond percolation model, where only two kinds of bonds (e.g., conducting and insulating bonds,  $\sigma_A = 1, \sigma_B = 0$ ) are considered. The analogous construction for three dimensions is obvious.

Clearly, the experimental situation described above requires  $\sigma_A / \sigma_B = \tau \gg 1; \sigma_C = 0$ . It is natural to assume that  $\sigma_A$  and  $\sigma_B$  are thermally activated, such that their ratio  $\tau \sim \exp(-\Delta E / k_B T)$  increases with decreasing temperature.

A remarkable feature of this model is the existence of two threshold concentrations. At  $p = p'_c$ , interface percolation (i.e., percolation of A bonds) sets in, whereas at  $p = p''_c = 1 - p'_c$  (normally not accessible by experiment) the system undergoes a conductor-insulator transition. The first critical concentration  $p'_c = 0.097$  corresponds to the threshold for third-neighbour site percolation on a 3-dimensional lattice.

Figure 5 shows the total conductivity obtained by Monte Carlo simulations [9,10], for three different temperatures (corresponding to  $\tau = 10, 30$  and  $100$ ). Good agreement with the experimental curves [11] is achieved, which show a broad maximum in the conductivity as a function of  $p$  in the range between the two thresholds. We like to note that the model also describes successfully the variation of the total conductivity with the size of the dispersed particles [12]. In particular, it was found that as the particle size decreases

while the thickness of the highly conducting interfacial layer is fixed, the maximum in the total conductivity as a function of the insulator concentration  $p$  shifts to smaller values of  $p$ . The observation of conductivity maxima at very low volume fractions close to 0.1 in certain composite electrolytes, however, was interpreted recently by a grain boundary mechanism within the bulk of the electrolyte phase [13].

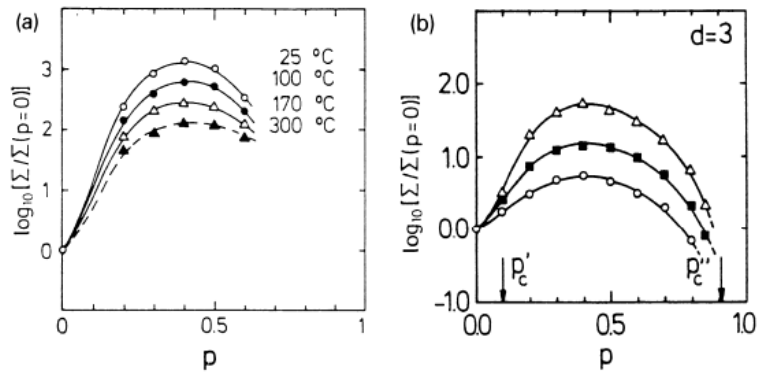


Fig. 5. (a) Normalized conductivity of the  $\text{LiI}-\text{Al}_2\text{O}_3$  system as a function of the mole fraction  $p$  of  $\text{Al}_2\text{O}_3$  at different temperatures (after [11]). (b) Normalized conductivity resulting from Monte Carlo simulations of the three-component percolation model, as a function of  $p$ , for  $\sigma_A^0/\sigma_B^0 = 10$  (circles), 30 (full squares), and 100 (triangles) (after [10]).

#### 4.2 Composite Micro- and Nanocrystalline Conductors

In the foregoing subsection, we have discussed dispersed ionic conductors that were prepared by melting the ionic conductor and adding the insulator (mainly  $\text{Al}_2\text{O}_3$ ) to it. Next we consider diphasic micro- and nanocrystalline materials, which were prepared by mixing the two different powders and pressing them together to a pellet. This way, in contrast to the classic dispersed ionic conductors discussed above, the grain size of both ionic conductor and insulator can be varied over several orders of magnitude. For reviews on nanocrystalline materials see, e.g., [13-16].

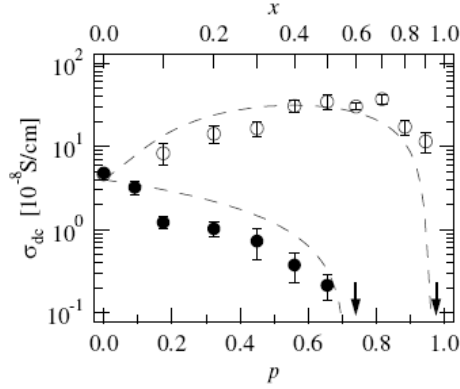


Fig. 6. Plot of the dc conductivity of microcrystalline (full circles) and nanocrystalline  $(1-x)\text{Li}_2\text{O}:x\text{B}_2\text{O}_3$  composites (open circles) vs volume fraction  $p$  (bottom scale) and mole fraction  $x$  (top scale) of insulating  $\text{B}_2\text{O}_3$ , at  $T = 433$  K. The arrows indicate the compositions where the dc conductivities fall below the detection limit. The dashed lines show the dc conductivities obtained from the continuum percolation model discussed in the text (after [18]).

Figure 6 shows the ionic conductivity of micro- and nanocrystalline  $(1-x)\text{Li}_2\text{O}:x\text{B}_2\text{O}_3$  composites for different contents  $x$  of insulator  $\text{B}_2\text{O}_3$  [17,18]. For pure  $\text{Li}_2\text{O}$ , i.e.  $x = p = 0$ , the dc conductivity of the microcrystalline and the nanocrystalline samples coincide. When  $\text{Li}_2\text{O}$  is successively substituted by  $\text{B}_2\text{O}_3$ , the two systems behave very different. In the microcrystalline samples, the dc conductivity decreases monotonically with  $x$ , while in the nanocrystalline samples, the dc conductivity first increases and reaches a maximum near  $x = 0.6$ , where the conductivity is about one order of magnitude larger than that of pure  $\text{Li}_2\text{O}$ . Further increase of the insulator content leads to a decrease of the conductivity. At  $x = 0.95$ , finally, the conductivity has dropped below the detection limit. As for the composites discussed above, the overall behaviour (including the differences between nano- and microcrystalline samples) can be explained assuming an enhanced conductivity at the interfaces between unlike grains. Even more remarkable than the increase of the dc conductivity with increasing insulator content, however, is the fact that, starting from the pure insulator  $\text{B}_2\text{O}_3$ , only a tiny volume fraction of  $\text{C}$  is needed to obtain a dc conductivity which is considerably higher than the dc conductivity of pure  $\text{Li}_2\text{O}$ .

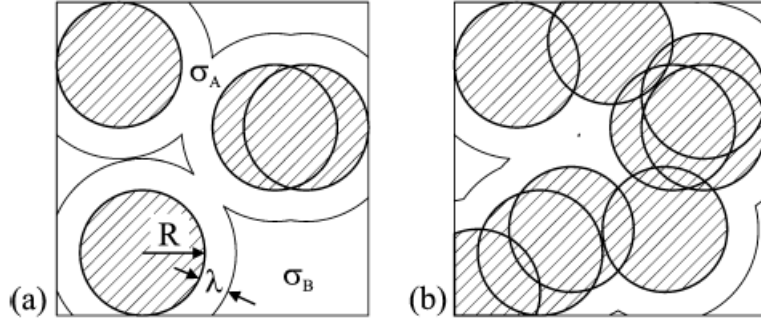


Fig. 7. Continuum percolation model with insulating spheres (radius  $R$ ) dispersed in an ionic conductor and a highly conducting interface, after [20]. The figures show the two critical insulator contents where (a) an infinite highly conducting pathway is formed and (b) this pathway is disrupted.

#### 4.3 Continuum percolation model

The increase of the ionic conductivity at intermediate insulator contents for the nanocrystalline composites clearly shows that the interfaces between the two components are responsible for the conductivity enhancement. To describe the dependence of the dc conductivity of the composites on the insulator content  $p$ , we first consider a continuum percolation model [19,20], which is sketched in Fig. 7. The insulating particles are represented by spheres with radius  $R$ . Around these insulating particles a highly conducting interface with width  $\lambda$  and ionic conductivity  $\sigma_A$  is created. The remaining volume represents the ionically conducting phase which has a conductivity  $\sigma_B$ . An enhancement factor  $\tau = \sigma_A/\sigma_B$  of 100 and an interface thickness  $\lambda = 1$  nm are assumed. The grain radii  $R$  have been determined by transmission electron microscopy and X-ray diffraction [21,22] and are roughly  $5 \mu\text{m}$  for the microcrystalline composites and  $10$  nm for the nanocrystalline composites. The overall conductivity of the system, calculated by an effective medium approximation [17], is shown in Fig. 6 (dashed curves). A good overall agreement with the experimental data is found. However, the effective coordination numbers  $z$  used in this approach as fit parameters to reproduce the experimental results ( $z = 7$  for the microsystem and  $z = 59$  for the nanosystem) can hardly be rationalized.

#### 4.4 Brick-layer type percolation model

In an attempt to understand the experimental results on a more microscopic basis, we next consider a brick-layer type model where both, micro- and nanocrystalline composites are treated on the same footing [23]. In the model, one starts with a cubic box of size  $L^3$  that is divided into a large number of small cubes with equal volumes  $a^3$ . Each of the small cubes is regarded as a grain of the composite. With a given probability  $p$  the cubes

are supposed to be insulating  $B_2O_3$  grains. Thus the volume fraction of the  $Li_2O$  grains is  $1 - p$ . By definition, conducting grains are connected when they have one corner in common. Fig. 8(a) shows the largest cluster of  $Li_2O$  grains that connects opposite faces of the large box close to the percolation threshold, at  $p = 0.9$ . Again a highly conducting interface of width  $\lambda$  between insulating and ionically conducting particles is assumed. Next the small cubes in Fig. 8(a), that represent the  $Li_2O$  grains, are replaced by a bond lattice sketched in Fig. 8(b). The bonds represent the ionic conduction (i) inside the grain ( $\Sigma_0$ ), (ii) along the interface area ( $\Sigma_1$ ) and (iii) along the interface edges ( $\Sigma_2$ ). The length of each bond is  $a/2$ . The cross section each bond represents is  $(a - \lambda)^2$  for the  $\Sigma_0$  bonds,  $(a - \lambda)\lambda$  for the  $\Sigma_1$  bonds and  $\lambda^2$  for the  $\Sigma_2$  bonds. Having this in mind, the conductance of each bond can be calculated easily. It is assumed that (i) in the bulk of the insulating  $B_2O_3$  grains, the specific conductivity is zero, that (ii) in the bulk of the conducting  $Li_2O$  grains as well as in the interfaces between them, the specific conductivity is  $\sigma_B$ , and that (iii)  $Li_2O$  grains in contact with a  $B_2O_3$  grain share a highly conducting interface with specific conductivity  $\sigma_A = \tau\sigma_B$ . The enhancement factor  $\tau$  is assumed to be of the order of  $10^2 - 10^3$ .

Finally, for calculating the total conductivity of the composite the problem is mapped onto the corresponding diffusion problem by defining appropriate jump rates (proportional to the bond conductances) along the bonds. For given values of  $\tau$ ,  $a$ ,  $\lambda$  and  $p$ , the mean square displacement  $\langle r^2(t) \rangle$  of many random walks is then determined as a function of time  $t$  on the largest cluster of each model system. Averaging over all of them, one obtains the diffusion coefficient  $D = \lim_{t \rightarrow \infty} \langle r^2(t) \rangle / 6t$ , which is proportional to the dc conductivity (cf. Eq. (9)).

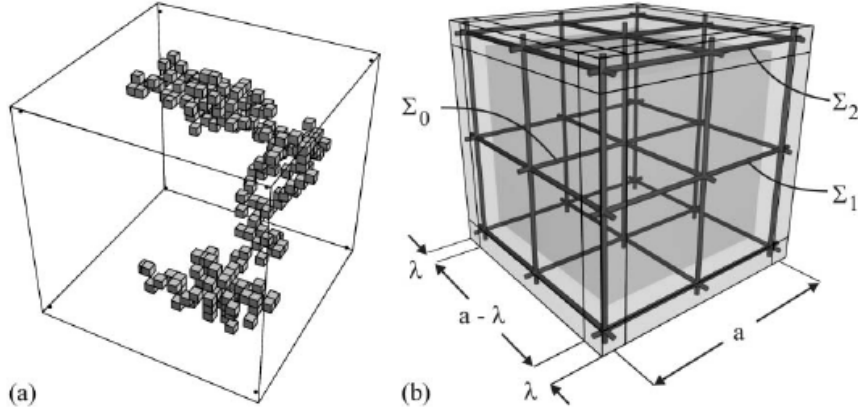


Fig. 8. (a) The largest cluster of insulating particles for the brick-layer type model in three dimensions at the critical concentration. (b) A single grain and the bonds assigned to conduction in the interior of the grains, along the sides and along the edges of the grain, after [23].

The numerical results for the dc conductivity *vs.* insulator volume content *p* are shown in Fig. 9 for various grain sizes *a* and enhancement factors  $\tau$ . In all model calculations, a fixed interface thickness  $\lambda = 1$  nm was assumed. The figure shows that this microscopic model, which treats nano- and microcrystalline samples in exactly the same way (the only difference is the size of the grains) is able to reproduce all qualitative features of the experimental results. One feature cannot be reproduced by the model, however, namely the very high insulator concentration where the conductivity drops to zero. We will come back to this point at the end of the next section.

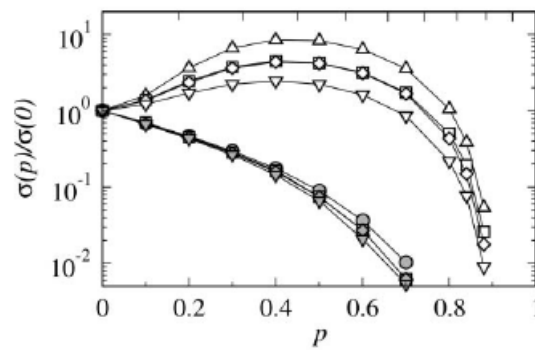


Fig. 9. Numerical results of the normalized dc conductivity  $\sigma(p)/\sigma(0)$  *vs.* insulator volume fraction *p* in the brick-layer type percolation model for different grain sizes *a* and enhancement factors  $\tau = \sigma_A/\sigma_B$ . In all cases the interface thickness  $\lambda = 1$  nm is fixed. Nanocrystalline grains:  $\Delta$  *a* = 10 nm,  $\tau = 200$ ;  $\square$  *a* = 10 nm,  $\tau = 100$ ;  $\diamond$  *a* = 20 nm,  $\tau = 200$ ;  $\nabla$  *a* = 20 nm,  $\tau = 100$ ; Microcrystalline grains:  $\bullet$  *a* = 10  $\mu\text{m}$ ,  $\tau = 200$ ;  $\blacksquare$  *a* = 10  $\mu\text{m}$ ,  $\tau = 100$ ;  $\blacklozenge$  *a* = 20  $\mu\text{m}$ ,  $\tau = 200$ ;  $\blacktriangledown$  *a* = 20  $\mu\text{m}$ ,  $\tau = 100$  (after [23]).

#### 4.5 Voronoi construction

To get a more realistic structure of the composites in the model description (compared to the over-simplified cubic arrangement) a Voronoi approach [24] has been used, see Fig. 10 for a two-dimensional sketch [18]. 2000 seeds which represent the centers of the grains have been

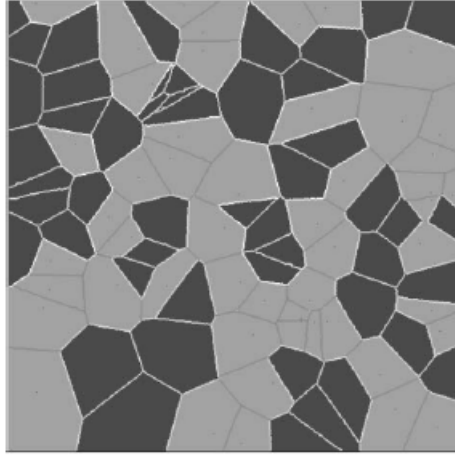


Fig. 10. Polycrystalline composite material created by Voronoi construction in two dimensions. Dark grey areas represent the ionic conductor grains and light grey areas represent the insulator grains, after [18].

placed randomly inside a volume of  $150^3$  lattice sites. The borders of the grains are defined by the planes perpendicular to the connection line between two neighbored seeds intersecting this line exactly in the middle between both seeds. By this a fully compacted structure of irregular polyhedra is created. The shapes of the individual grains differ significantly and thus the number of edges of a crystallite does also change which results in a locally varying coordination number. Furthermore the particles are not mono-disperse but show a distribution of grain sizes. The distribution of the local coordination numbers of the Voronoi system is a Gaussian, with an average coordination number close to 15.6 and a standard deviation close to 4.4. The grain volumes follow a log-normal distribution, in agreement with the experimental situation.

The structure created by the Voronoi construction seems to represent quite nicely a real polycrystalline material (though pores are not included). The cells in Fig. 10 can now be regarded as insulating with probability  $p$  and as ionically conducting with probability  $(1 - p)$ , irrespective of their size.

It is clear that the dc conductivity will show a similar behaviour as in the two models before. The main question that arises is whether the more realistic Voronoi construction is able to describe the conductivity close to  $p = 1$  in a better manner than the previous models. To this end, the percolation probability  $P(p)$  for ionically conducting particles to percolate the system was determined. The result is shown in Fig. 11. One can see that the critical concentration  $p_c$  above which the conducting paths get disrupted is close to 0.86, being even smaller than the value which was obtained for the brick-layer model in the foregoing section.

A reason for this underestimation of  $p_c$  might be that Li ion transport is also possible in the interface between insulating nanocrystalline grains, representing an additional Li diffusion passageway of nanometer length. Indeed, the percolation threshold increases to about 0.93 (see Fig. 11) if  $B_2O_3/B_2O_3$  interfaces are considered to be permeable for Li ions (thus linking two nondirectly connected  $Li_2O$  grains) if the length of these interfaces is smaller than the average particle diameter. In the brick-layer model, the assumption of such a ‘nanometer-passageway diffusion’ yields a threshold close to 0.95 [23].

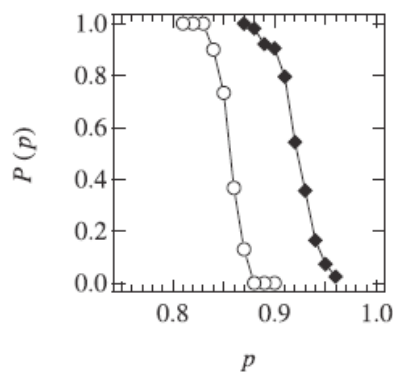


Fig. 11. The percolation probability  $P(p)$  of the ionically conducting particles vs. insulator volume fraction  $p$  in the three-dimensional Voronoi system shown as white circles. The black squares represent the case where Li ions can pass along  $B_2O_3/B_2O_3$  interfaces being shorter than the average grain diameter, after [18].

We gratefully acknowledge very valuable discussions with Wolfgang Dieterich, Joachim Maier, and H. Eduardo Roman.

## References

- [1] Fractals and Disordered Systems, ed. by A. Bunde, S. Havlin (Springer, Berlin, 1996)
- [2] D. Stauffer, A. Aharony: Introduction to Percolation Theory (Taylor & Francis, London, 1992)
- [3] M. Sahimi: Application of Percolation Theory (Taylor & Francis, London, 1994)
- [4] S. Alexander, R.L. Orbach: J. Phys. Lett. (Paris) **43**, L625 (1982)
- [5] S. Feng, B.I. Halperin, P. Sen: Phys. Rev. B **35**, 197 (1987)
- [6] C.C. Liang: J. Electrochem. Soc. **120**, 1289 (1973)
- [7] For a review see: A.K. Shukla, V. Sharma. In: Solid State Ionics: Materials Applications, ed. by B.V.R. Chowdari, S. Chandra, S. Singh, P.C. Srivastava (World Scientific, Singapore 1992) p. 91
- [8] J. Maier. In: Superionic Solids and Electrolytes, ed. by A.L. Laskar, S. Chandra (Academic Press, New York 1989) p. 137

- [9] A. Bunde, W. Dieterich, H.E. Roman: *Phys. Rev. Lett.* **55**, 5 (1985)
- [10] H.E. Roman, A. Bunde, W. Dieterich: *Phys. Rev. B* **34**, 3439 (1986)
- [11] F.W. Poulsen, N.H. Andersen, B. Kinde, J. Schoonman: *Solid State Ionics* **9/10**, 119 (1983)
- [12] H.E. Roman, M. Yussou: *Phys. Rev. B* **36**, 7285 (1987)
- [13] H. Gleiter: *Progress in Materials Science* **33**, 223 (1989)
- [14] R.W. Siegel: *Nanophase Materials*. In: *Encyclopedia of Applied Physics*, vol. 11, ed. by G.L. Trigg, E.H. Immergut, E.S. Vera, W. Greulich (VCH, New York, 1994) pp. 173-200
- [15] J. Maier: *Prog. Solid State Chem.* **23**, 171 (1995)
- [16] P. Heitjans, S. Indris: *J. Phys.: Condens. Matter* **15**, R1257 (2003)
- [17] S. Indris, P. Heitjans, H.E. Roman, A. Bunde: *Phys. Rev. Lett.* **84**, 2889 (2000)
- [18] S. Indris, P. Heitjans, M. Ulrich, A. Bunde: *Z. Phys. Chem.* **219**, 89 (2005)
- [19] A. G. Rojo, H. E. Roman, *Phys. Rev. B* **37**, 3696 (1988)
- [20] H. E. Roman, *J. Phys.: Condens. Matter* **2**, 3909 (1990)
- [21] S. Indris, P. Heitjans, *Mater. Sci. Forum* **343–346**, 417 (2000)
- [22] S. Indris, D. Bork, P. Heitjans, *J. Mater. Synth. Process.* **8**, 245 (2000)
- [23] M. Ulrich, A. Bunde, S. Indris, P. Heitjans, *Phys. Chem. Chem. Phys.* **6**, 3680 (2004)
- [24] A. Okabe, B. Boots, K. Sugihara, *Spatial Tessellations: Concepts and Applications of Voronoi Diagrams*, Wiley, Chichester, 1992.